

# A STANDARD DT SUPERSHOT SIMULATION

R.V. BUDNY  
 Plasma Physics Laboratory,  
 Princeton University,  
 Princeton, New Jersey,  
 United States of America

**ABSTRACT.** A simulation of an anticipated TFTR deuterium–tritium supershot is described. The simulation is based on a reproducible, high performance, long duration D-only supershot. The TRANSP plasma analysis code is used to model fast ion (D, T and alpha) parameters, including their distributions in energy and pitch angle.

## 1. INTRODUCTION

Experiments with deuterium–tritium (DT) supershots were scheduled for TFTR starting in the fall of 1993. A large number of DT simulations have been performed by using the TRANSP plasma analysis code for designing experiments and diagnostics, and for alpha physics studies. Examples based on discharges from 1986 to 1990 have been published [1]. The purpose of this paper is to provide more detailed simulations based on a more recent supershot. Distributions of the fast ions in energy and pitch angle are given.

One of the simulations discussed in Ref. [1] (based on 55 851) had been selected as a standard example and has been used for theoretical studies of TAE modes [2]. The absence of significant MHD activity in this discharge made it appear especially suitable for DT experiments since the coherent MHD activity, which is often observed in supershots, may increase the alpha transport and prevent the accumulation of significant alpha pressures. MHD activity may also spoil the reproducibility, making it more difficult to study the alpha physics.

An experiment was conducted to optimize long duration, high performance supershots for reproducibility [3, 4]. The lithium pellet limiter conditioning that was used for 55 851 was not used for this experiment. Although lithium pellet conditioning improves the energy confinement and increases the neutron emissivity, it appears to reduce the reproducibility. The optimum discharges found in this experiment had less beam power and neutron yield than 55 851, but were more reproducible. These supershots also have lower central pressure and  $\beta$  and thus appear to have more margin to accommodate the higher pressure expected in DT owing to differences in T neutral beam injection (NBI), the additional alpha pressure, and the higher electron temperature from the alpha heating.

Many examples of these moderate, long duration, high performance supershots have been collected. Typically, they have ‘benign’ fishbone activity [5] during the flat-top phase. One of them with average performance, 66 887, was chosen as a new standard for simulations. Parameters during the relatively stationary phase of NBI ( $\sim 3.5$ – $4.0$  s) are:  $P_B = 24.4$  MW,  $I_p = 1.65$  MA,  $B_{TF} = 4.76$  T,  $R_0 = 2.45$  m,  $a = 0.8$  m,  $q_\psi(0) \approx 0.9$ , and  $q_\psi(a) = 5$ .

TABLE I. COMPONENTS OF STORED ENERGY FOR THE DD AND DT SUPERSHOTS

	DD (66 887 A08) (MJ)	DT (66 887 P10) (MJ)
$U_{\text{total}}$	3.42	3.69
$U_{\text{par}}$	0.70	0.80
$U_{\text{prp}}$	0.91	1.08
$U_e$	0.91	0.93
$U_{\text{ion}}$	0.89	0.88
$U_\alpha$	0.00	0.15

TABLE II. COMPONENTS OF VOLUME AVERAGED BETA FOR THE DD AND DT SUPERSHOTS

	DD (66 887 A08) (%)	DT (66 887 P10) (%)
$\langle \beta_{\text{total}} \rangle$	0.783	0.842
$\langle \beta_{\text{beam}} \rangle$	0.370	0.395
$\langle \beta_e \rangle$	0.208	0.213
$\langle \beta_{\text{ion}} \rangle$	0.205	0.202
$\langle \beta_\alpha \rangle$	0	0.034

The total and thermal energy confinement times are 0.14 s and 0.087 s, respectively. The components of the volume integrated stored energies at 3.75 s are given in Table I. The volume averages of the components of toroidal beta are listed in Table II. The definition of the local toroidal beta used here is the pressure divided by  $8\pi\langle B_z^2 \rangle$ , where  $\langle \dots \rangle$  is the volume average and  $B_z$  is the vacuum toroidal field. The value of  $8\pi\langle B_z^2 \rangle$  is  $9.28 \text{ MJ/m}^3$ . The pressure terms are 1.5 times the energy densities of the electrons, thermal ions, or parallel plus perpendicular fast ions. The sum of these defines the total toroidal  $\beta_{\text{total}}$ . The peak value of  $\beta_{\text{norm}} \equiv \langle \beta_{\text{total}} \rangle / I_p / aB_{\text{TF}}$  is 1.85.

The values of the central  $Z_{\text{eff}}$  decrease to  $\approx 2\text{--}3$  during the NBI phase. The impurities consist of carbon and small traces of metals. The contribution to the central  $Z_{\text{eff}}$  from metals is less than  $\approx 0.02$ . The average charge of the impurities in this discharge is  $\approx 6.05$ . The total particle confinement time is modelled to be approximately 0.07 s.

## 2. TRANSP CODE

The TRANSP plasma analysis code has several modes of operation. Although its main use is for the analysis of tokamak discharges using measured parameters, it also can be used in predictive modes. The analysis mode provides information on the consistency of measured parameters and calculates parameters which are difficult to measure directly. Examples of the latter are the profiles of the plasma currents, the fast ion densities and pressures from NBI or ICRF heating or from fusion reactions, and the particle and energy transport.

Minimal assumptions and few adjustable parameters can be used for TRANSP modelling. Assumptions that are typically used for modelling TFTR supershots are that the  $Z_{\text{eff}}$  profiles are flat, that the parallel resistivity, the magnetic field diffusion and the fast ion orbits are neoclassical, and that the heat convection multipliers for the ions and electrons are  $3/2$ . The measured time dependent profiles of  $n_e$ ,  $T_e$ ,  $T_{\text{imp}}$  (the impurity temperature) and  $v_\phi$  (the toroidal rotation) are used. TRANSP calculates the hydrogenic temperature, denoted  $T_D$ , from  $T_{\text{imp}}$  [1]. This temperature is considerably lower than  $T_{\text{imp}}$  at the centre of the discharge during the first 0.2 s of NBI. Later, the difference decreases to several keV at the centre. This  $T_D$  is used to model the D-only discharge and to simulate the DT discharge. For example,  $T_D$  is used in the cross-sections and in the ion thermal energy.

In various predictive modes, transport coefficients can be assumed, and consequences such as profiles of temperatures and currents can be calculated. One of these

predictive modes is used for the DT predictions given below.

Recently, the number of non-impurity thermal ion species that can be modelled in TRANSP has been increased from three to five. One impurity species can be, and generally is, modelled. Fast ion parameters can be calculated by using either Monte Carlo or Fokker–Planck techniques. Most of the results to be discussed below are calculated with the Monte Carlo option, but some results from the Fokker–Planck option are also discussed and compared. With the Monte Carlo option [6], three fast species (beam ions and/or fusion products) can be modelled. The fast ions are treated as thermalized when they slow down to the average energy of the local thermal ion population ( $\frac{3}{2}T_i$ ).

With the Fokker–Planck option [7], only two species (beam ions) are modelled. This option, formulated by G. Hammett, uses a bounce averaging technique [8]. He recently improved the thermalization model to give a more realistic simulation. For this purpose, he rewrote the Fokker–Planck equation as

$$\frac{df}{dt} = S_{\text{fast}} + C_i(f) + C_e(f) - \frac{f}{\tau_{\text{cx}}} - S_{\text{orbit}} - \frac{f_{\text{Maxwell}}}{\tau_{\text{therm}}} H(4T_i - E)$$

where  $f$  is the distribution of either of the beam ions (excluding the thermal contribution),  $S_{\text{fast}}$  is the fast ion source rate,  $C_i$  the collision operator with thermal ions, and  $C_e$  the collision operator with electrons.  $S_{\text{orbit}}$  is the loss of particles into unconfined orbits.

The thermalization time  $\tau_{\text{therm}}$  is chosen to be as short as possible while maintaining  $f$  positive everywhere. The Heaviside function  $H(4T_i - E)$  guarantees that the only particles thermalized are those with  $E < 4T_i$  or less if the loss cone extends to an energy of less than  $4T_i$ . This later case is unlikely, but might happen in pathological cases near the edge. The inclusion of the Heaviside function is necessary since only the isotropic  $f_{\text{Maxwell}}$  is subtracted from  $f$  in each time step. At high energies the pitch angle scattering rate is very low, which implies that it takes a long time to isotropize. Without the Heaviside function,  $\tau_{\text{therm}}$  would be very long. Furthermore, at very high energies  $f$  is distorted by loss cones and by collisions with electrons (which causes  $f$  to have a slope above the critical energy of  $T_e$ , not  $T_i$ ); so blindly subtracting off  $f_{\text{Maxwell}}$  with a  $T_i$  slope would result in negative values for  $f$  unless  $\tau_{\text{therm}}$  were very large.

This thermalization method is superior to that used by the Monte Carlo option since instantly rendering the fast ions to thermal at  $\frac{3}{2}T_i$  ignores the fact that it takes an ion–ion collision to isotropize the ions. However, the

Monte Carlo option does a better job of handling other physics details, as the Fokker-Planck option provides no reabsorption of charge exchanged ions and uses a small banana width approximation for the fast ions.

The alpha particle distributions are simulated with the Monte Carlo option only. The alpha births are performed by using spatially 2D fusion reaction rate data (beam-beam + beam-target + thermonuclear) computed in the preceding time step. The alpha particles are launched isotropically in the (rotating) plasma frame with the appropriate birth energy ( $E_0 = 3.5$  MeV). This had previously been incorrectly coded in TRANSP, resulting in too many alphas being launched with pitch angles  $\lambda$  ( $\equiv v_{\text{par}}/v$  with  $v_{\text{par}}$  the parallel component of the velocity  $v$ ) near  $-1$  or  $+1$ . The main effects of this were that the predictions of central alpha densities and  $\beta_\alpha$  were about 25% too high. This has been corrected in July 1993.

Effects of Doppler broadening of the alpha distributions from beam-target interactions have not yet been incorporated in TRANSP. The alpha orbits and slowing down, and their heating of the thermal plasma, are calculated by using the same Monte Carlo methods as are employed in modelling the fast ions from NBI. The model takes into account non-zero orbit width and Larmor radius effects, but magnetic field ripple effects are not included.

Ripple effects appear to be insignificant for  $R_0 = 2.45$  m plasmas. They are estimated to be  $<5\%$  [9]. Less than 10% of the alpha particles are expected to escape from the plasma via prompt first orbit loss if the plasma current is higher than  $I_p \approx 1.5$  MA [10]. Measured DD fusion product losses agree with first orbit and ripple loss model predictions in many cases [10, 11]. Anomalous diffusion of the fast ions can be modelled in TRANSP. The anomalous loss of beam ions is relatively small for plasmas with  $R_0 = 2.45$  m when the current is not small ( $I_p > 1$  MA) [12, 13]. If the beam ions in typical supershots had a constant anomalous diffusivity greater than  $\approx 0.2$  m<sup>2</sup>/s, the beam density would decrease sufficiently to lower the neutron emission and stored energy considerably below the measured values. No anomalous diffusivity is assumed in this paper.

The TFTR inner and outer (RF) limiters are modelled in TRANSP as toroidally symmetric circles. Trapped alphas are considered as lost to the limiters if their orbit guiding centres either come within a Larmor radius of these limiters or if the guiding centres extend past a flux surface located outside the last closed flux surface having the extrapolated value of the square root of the normalized toroidal flux,  $x$ , equal to 1.3. The actual flux surfaces outside the last closed flux surface are unknown to TRANSP, so that only approximate orbits are used in this

region. For this reason the extrapolation is not extended beyond  $x = 1.3$ . The actual outer (RF) limiter is beyond this surface for most plasmas with a major radius of 2.45 m; thus, TRANSP slightly overestimates the alpha orbit loss.

The alpha particles slow down and pitch angle scatter on thermal plasma species (electrons, ions and impurities). Collisional coupling between fast ion species (e.g. beam-beam and beam-alpha particle collisional effects) is not computed. The accumulation of thermalized alpha particles can be modelled with TRANSP by using the increased number of thermal ion species (using D, T, <sup>4</sup>He and an impurity species). The <sup>4</sup>He transport must be assumed.

### 3. D-ONLY SUPERSHOT MODELLING

The time evolutions of several parameters of the discharge are shown in Fig. 1. The TRANSP modelling is tested by comparing simulations with measurements. Examples of parameters that are compared are the total neutron emission rate, the total energy, the surface voltage, the neutron emission profile and the Shafranov shifts. These are compared in Figs 2 and 3. The total neutron emission, shown in Fig. 2(a), is approximately 20% below the measured rate. The one  $1\sigma$  error on the measurement is  $\approx 15\%$ . The total stored energy, shown in Fig. 2(b), is about 100 kJ above the value derived from magnetics measurements. The  $1\sigma$  for this measurement is  $\approx 80$  kJ. The surface voltage is compared in Fig. 2(c). The spikes in the measured voltage at the start and the termination of the NBI are due to feedback from the plasma control. The measured accuracy is  $\approx 1$  mV. The agreement is not very good, apparently because of the sensitivity to  $T_e$  in the plasma edge, which is not known very accurately.

The neutron emission profile is measured by a collimator array. An example of the measured and calculated profiles versus the major radius is shown in Fig. 3(a). The profiles are in approximate agreement throughout the NBI phase. Examples of TRANSP symmetrized density profiles are shown in Fig. 3(b). The electron density profile is measured by interferometer. The Shafranov shifts, calculated in TRANSP by using the kinetic pressure, is in close agreement with the measured profiles. Examples of TRANSP symmetrized temperature profiles are shown in Fig. 3(c). The temperature of the impurity ions is measured by using charge exchange spectroscopy of the carbon impurity. The temperature of the thermal D is calculated [1] from this impurity temperature. The electron temperature is calculated from electron cyclotron emission (ECE).

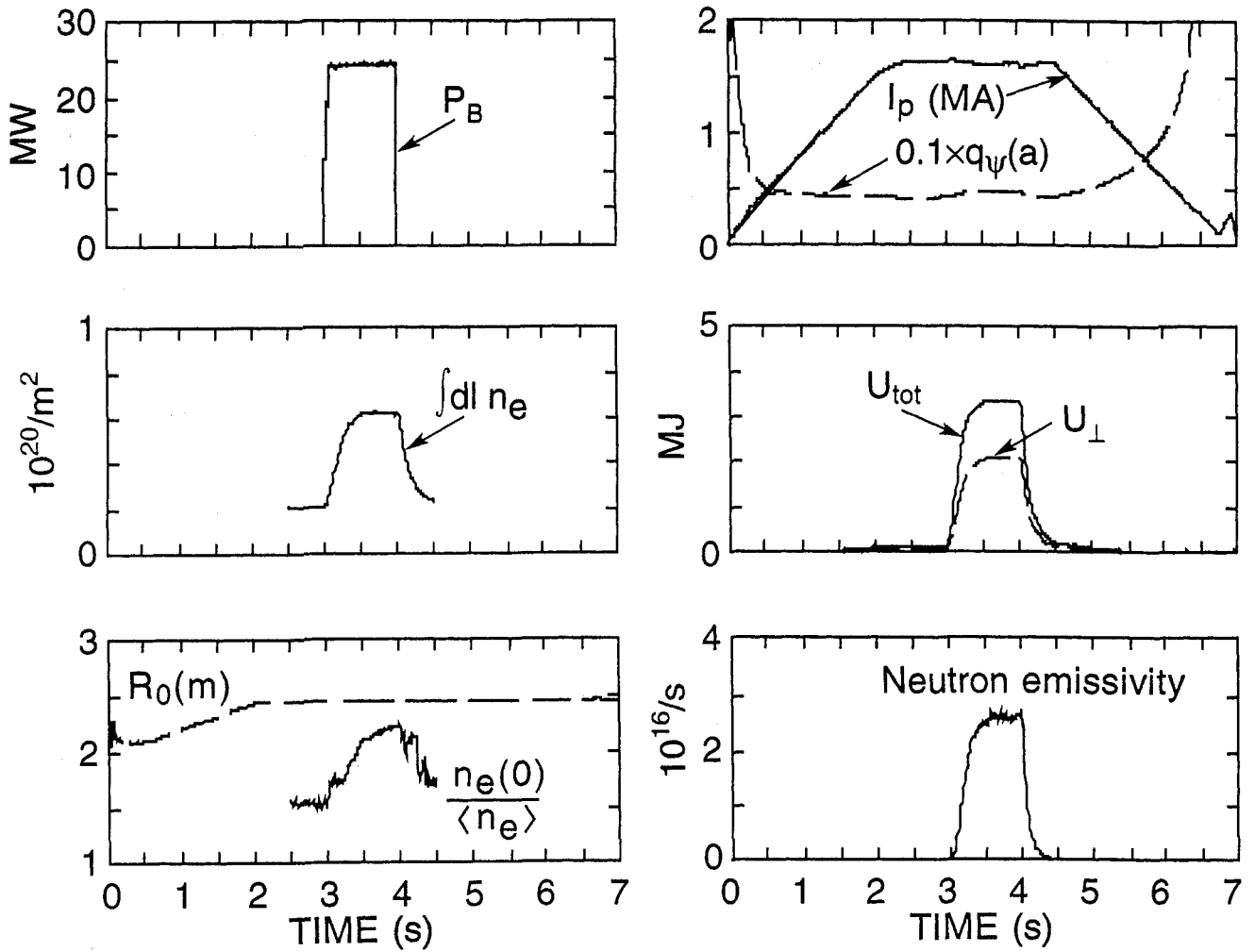
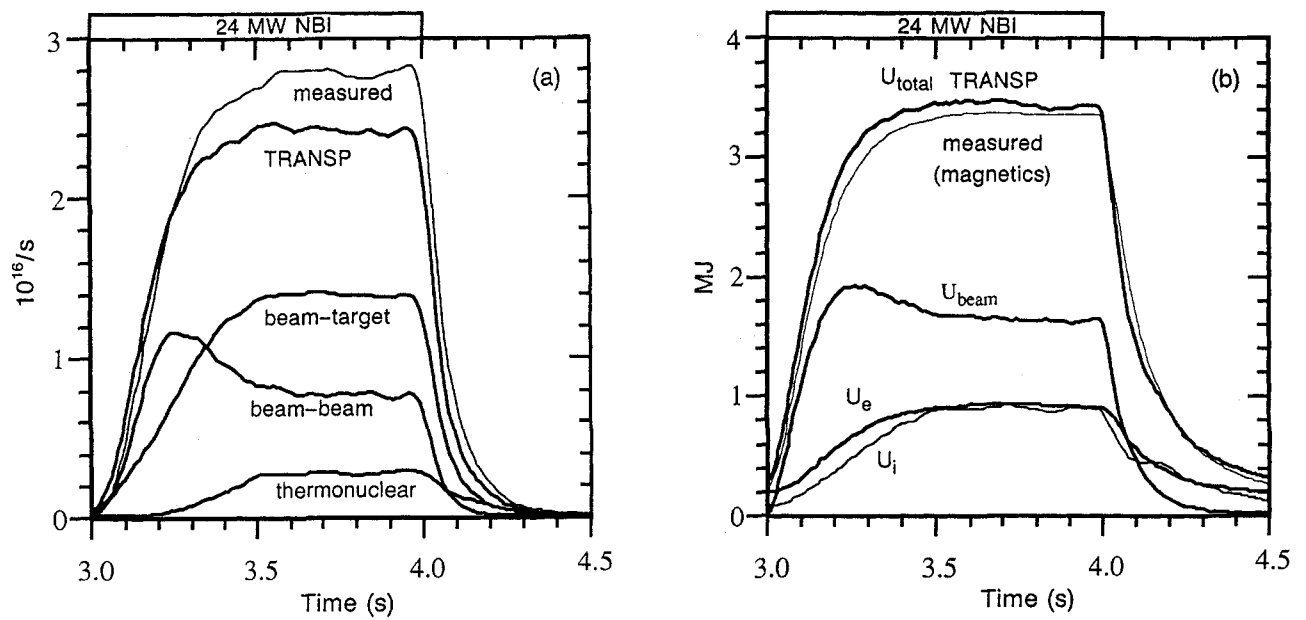


FIG. 1. Waveforms of 66 887 for applied NBI power, chordal density, density peakedness, major radius, current,  $q_\psi(a)$ , total and perpendicular stored energy, and total neutron emission.



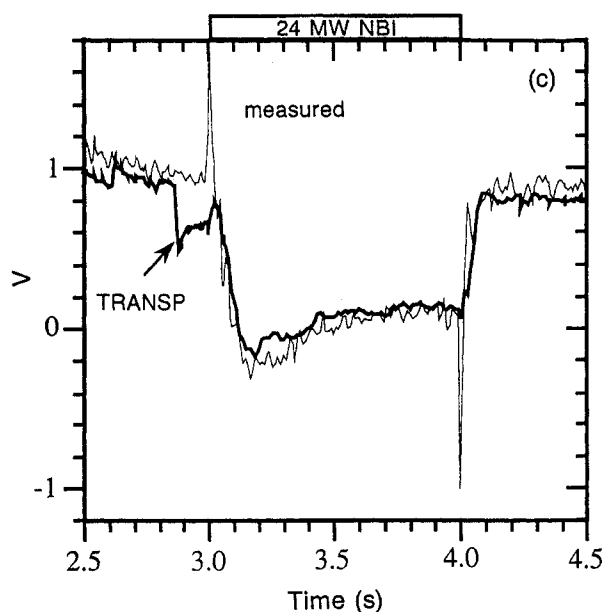


FIG. 2. Comparison of time evolutions of TRANSP simulations with measurements: (a) total neutron emission and the computed beam-target, beam-beam and thermal components; (b) total energy and energies of the plasma components; (c) surface voltage.

The ideal MHD high  $n$  stability of the discharge has been analysed [14] by using the EQGRUM [15] and STBAL [16] codes. The results indicate that the gradient of the total (thermal + beam ion) pressure could increase  $\approx 30\%$  before reaching the high  $n$  stability limit. Higher performance supershots are computed to be closer to the unstable region. An example (for 55 851) is shown in Ref. [1].

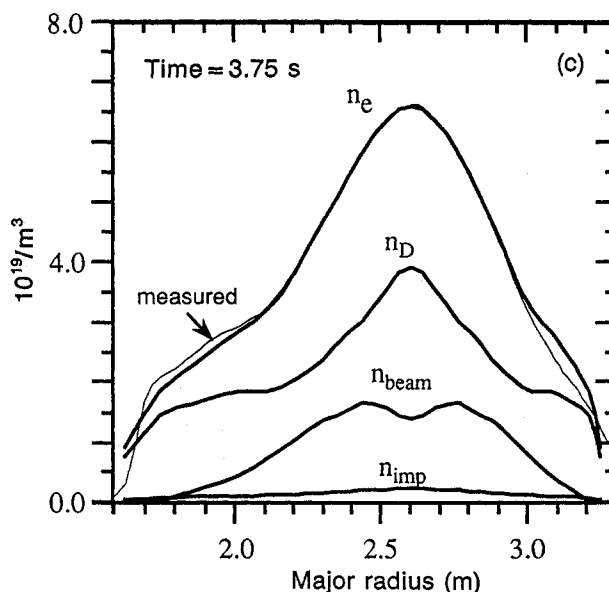
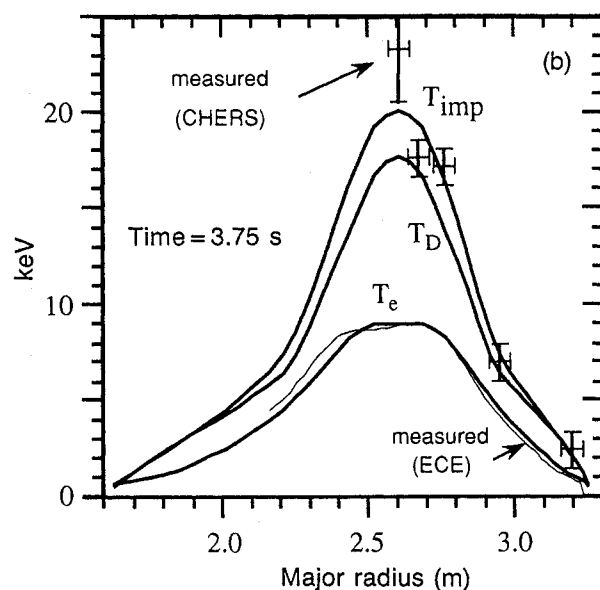
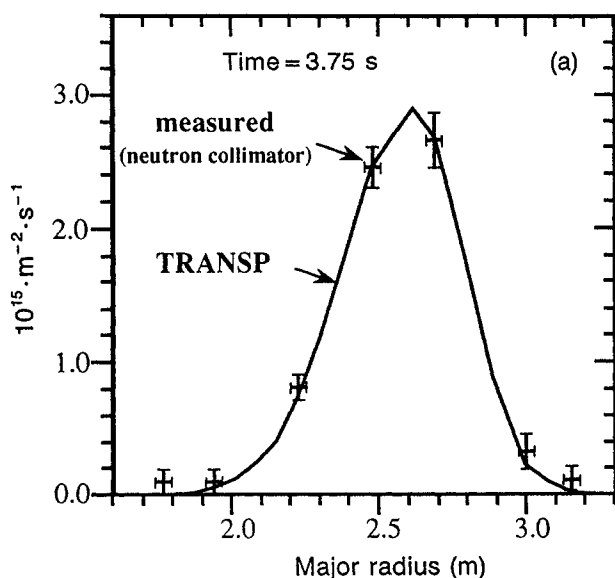


FIG. 3. Comparison of profiles from TRANSP simulations with measurements: (a) total neutron emission measured by a neutron collimator array; (b)  $T_e$  measured from electron emission,  $T_{imp}$  measured from charge exchange recombination spectroscopy, and  $T_D$  corrected for impurity hydrogenic differences; (c)  $n_e$  measured by interferometer, and  $n_D$ ,  $n_{beam}$  and  $n_{imp}$  calculated by TRANSP.

#### 4. DT SIMULATIONS

The TRANSP modelling for the D-only supershot, described in the previous section, agrees sufficiently well with measurements that the DT simulation should be a good estimate of the DT parameters to be expected.

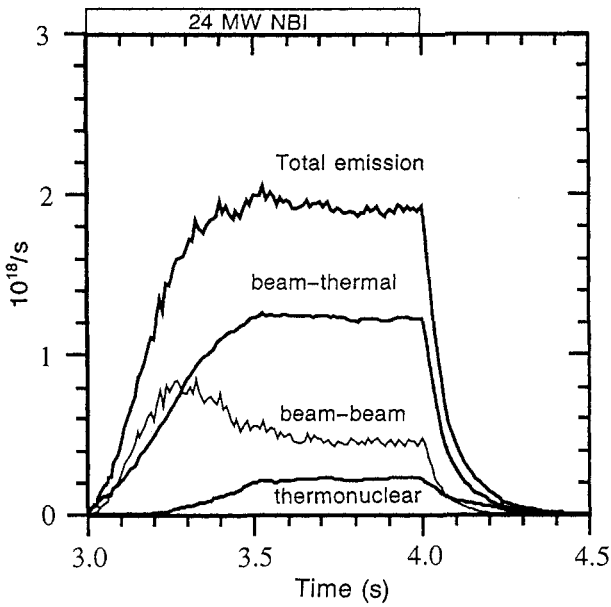


FIG. 4. Time evolution of total neutron emissivity and its components from beam-thermal, beam-beam and thermonuclear DT fusions predicted by using the Monte Carlo option.

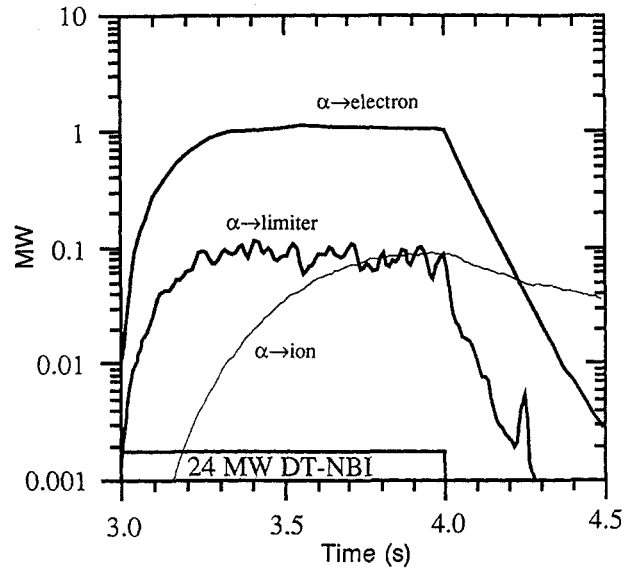


FIG. 5. Time evolution of loss of alpha power to limiters or by excursion past  $x = 1.3$ .

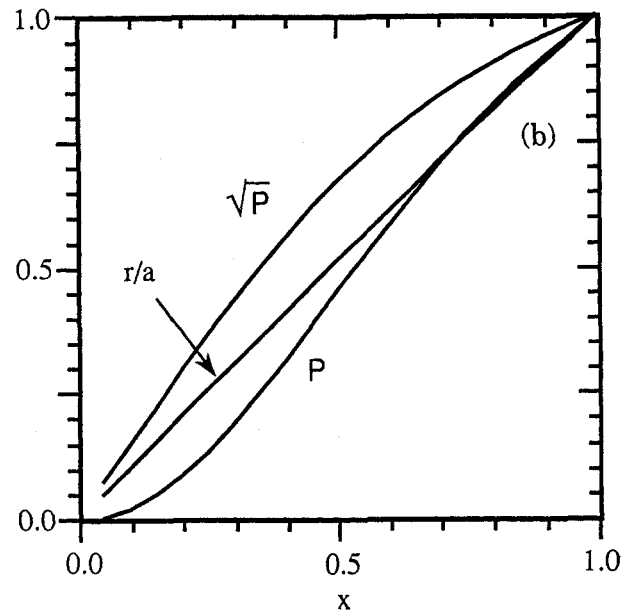
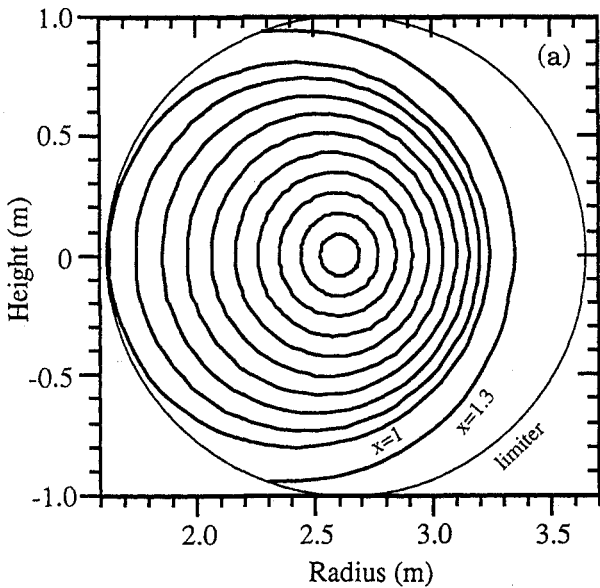


FIG. 6. (a) Toroidal slice through TFTR showing the circle which is the approximate location of the limiters and the MHD equilibrium flux surfaces calculated by TRANSP and parametrized by the square root of the normalized toroidal flux  $x = 0.2, 0.4, 0.6, 0.8, 1$  (the last closed flux surface), and 1.3, which is used as the cut-off for alpha orbits; (b) profile of  $r/a$ , the normalized poloidal flux  $P$ , and the square root of  $P$  versus  $x$ .

TFTR has twelve NBI sources, six aimed in the co-direction and the other six in the counter-direction; D or T can be injected in any combination of these sources. For the DT simulations discussed here, the NBI is assumed to consist of 13 MW D NBI from five sources and 11.4 MW T NBI from another five sources. The

injections of both the D and T are chosen to be nearly balanced (co versus counter). The voltages of the full energy components are chosen to be those of 66 887, approximately 105 keV. The half and third energy fractions are chosen to be approximately those of 66 887 also.

The neutron emissivity rates predicted by the Monte Carlo run are shown in Fig. 4. The thermonuclear fraction is 10% of the total. This fraction is predicted to be higher (up to  $\sim 30\%$ ) for supershots with higher central densities. The simulation yields peak values of the neutron emission rate,  $S_n = 2.0 \times 10^{18}/s$ , and the fusion power,  $P_{DT} (\equiv S_n/3.6 \times 10^{17} \text{ [MW/s]}) = 5.6 \text{ MW}$ . The normalized fusion yield is  $Q_{DT} (\equiv P_{DT}/P_B) = 0.23$ . The total and beam-target neutron emission rates predicted with the Fokker-Planck option are 35% higher. This option typically gives higher neutron rates since the beam density is computed to be higher in the plasma centre. This is largely due to the neglect of beam charge exchange recapture in the Fokker-Planck option. The more careful treatment of thermalization in the Fokker-Planck option discussed in the previous section does not have a large effect on the neutron emission compared with the standard treatment.

The time evolutions of the alpha heating and the alpha power lost to the limiter are shown in Fig. 5. The limiter loss is computed to be  $\sim 8\%$  of the alpha heating rate. A cross-section through the plasma showing flux surfaces and the location of the limiters is given in Fig. 6(a). Supershots generally have flux surfaces that are approximately circular, with  $x$  close in value to  $r/a$ . A plot of  $r/a$  versus  $x$  is given in Fig. 6(b).

Profiles of the classical estimates for the scattering times and slowing down times for the fast particles from birth to thermalization are shown in Fig. 7. Profiles of the

average energies of the fast ions are shown in Fig. 8. The density of the fast ions in the edge ( $x \approx 0.8-1.0$ ) is computed to be several orders of magnitude lower than their central values. The average energy of the fast ions has a minimum close to the edge and increases to relatively high values at the edge. This results in the prompt loss of these ions being more rapid than the scattering of lower energy ions into these regions. Thus, many of the ions at the edge have energies relatively close to their birth energies.

The electron temperature is expected to be affected by the alpha heating, by any intrinsic isotopic mass scaling, and by differences in the D and T NBI deposition and heating. Methods for separating these effects are discussed in Ref. [3]. For the simulations discussed here, the electron energy conductivity  $\chi_e$  is assumed to be identical with that calculated for the D-only supershot. The alpha-ion heating is calculated to be about 10% of the alpha-electron heating, and is neglected here. The  $T_D$  profiles computed for the D-only supershot are used for the DT modelling. This models the case where there is no intrinsic isotopic scaling difference between D-only and DT, and where there is no change in confinement with the increase in heating due to the alpha particles. The intrinsic isotopic scaling from D-only to DT supershots is unknown. The energy transport in supershots is insensitive to changes in the NBI power, but it is not known if this will be the case with alpha heating.

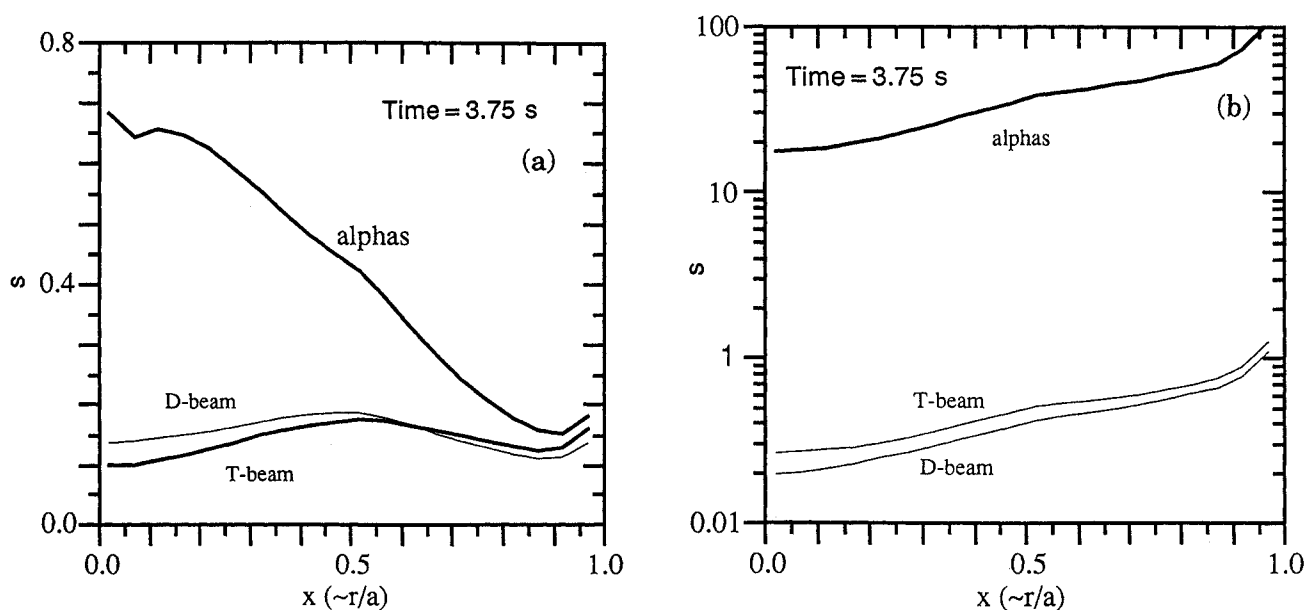


FIG. 7. Profiles versus square root of the normalized toroidal flux parameter  $x$  of the fast ion (a) slowing down times, and (b) scattering times at their birth energies. Local plasma parameters and classical expressions for the intersections are used for those plots. TRANSP uses Monte Carlo methods instead.

The net effect of this assumption of identical  $\chi_e$  for D-only and DT on the central  $T_e$  is that it is predicted to increase by  $\sim 10\%$  in DT. Profiles of the total pressure and electron temperature of the D-only supershot and of the DT simulation are compared in Fig. 9. Figure 9(c) shows that  $p'$  is expected to increase more than 20% in the inner third of the DT supershot relative to the D-only supershot. This increase is due to the increased electron energy, the beam energy and the additional alpha pressure, listed in Table I. The simulation yields the volume averages of the beta toroidal components shown in Table II. The value of  $\beta_{\text{norm}}$  is 1.99.

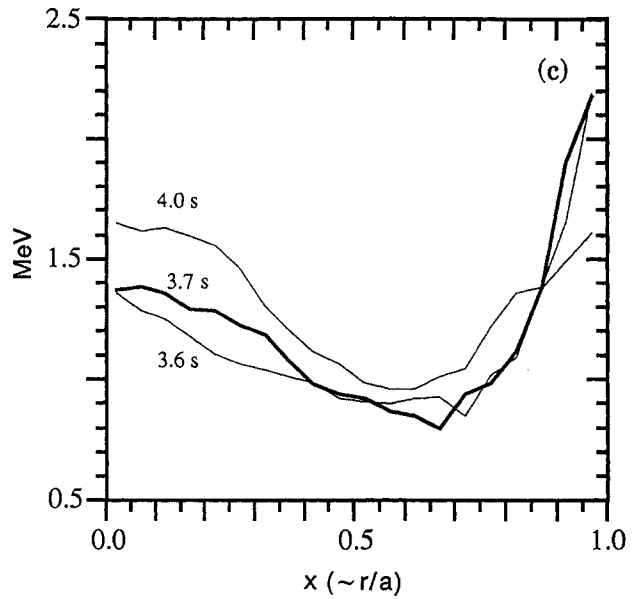
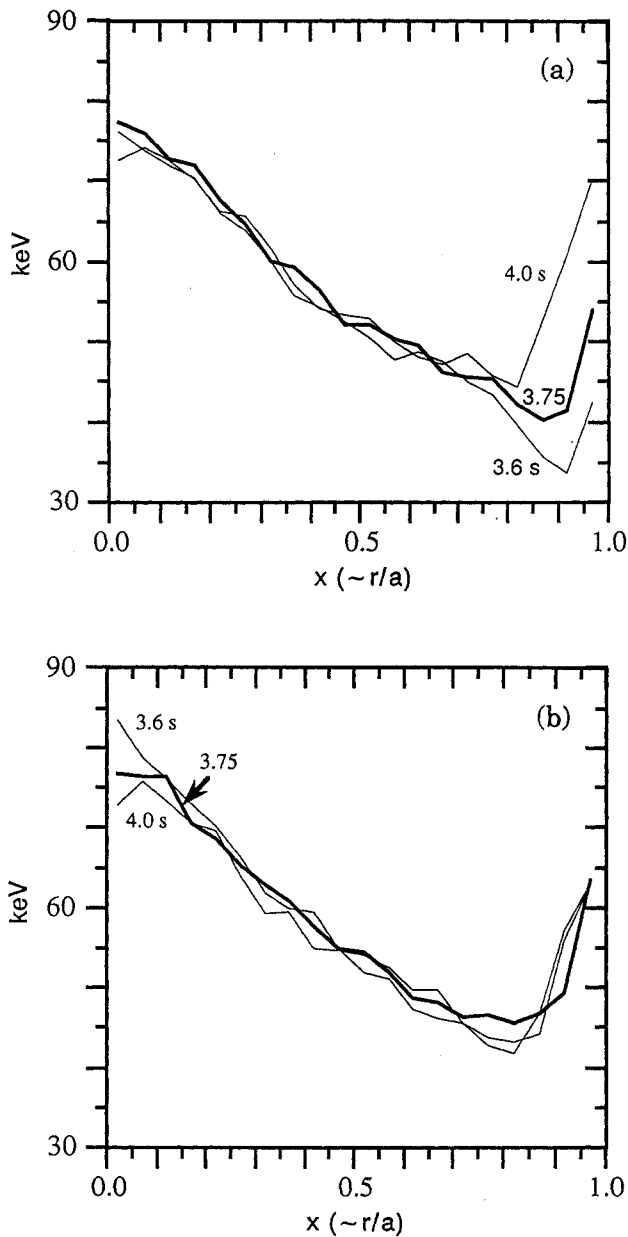


FIG. 8. Profiles of average energies of fast (a) D beam ions, (b) T beam ions, (c) alpha particles versus  $x$ . Profiles at several times are shown. The fast D and T ion profiles are relatively constant compared with those of the alphas.

The ideal MHD stability of the D-only supershot and of the DT simulation has been analysed [17] by using the PEST package [18]. Both are calculated to be unstable to an internal  $m = n = 1$  mode. Such a mode would be expected since the D-only supershot exhibited fishbone activity during the steady state phase of NBI.

The peakedness of some of the DT profiles is shown in Fig. 10. The neutron production rates, the fast alpha distribution, and  $\beta_\alpha$  are very peaked, relative to other profiles. TRANSP symmetrized density profiles are shown in Fig. 11(a). The thermal D and T densities differ considerably because of the different recycling. The TFTR limiter is assumed to be well conditioned, as is necessary for achieving supershots. This implies that the limiter will not have been loaded with tritium, and thus the recycling is expected to be dominated by deuterium influx. The profiles of components of  $\beta_{\text{tor}}$  are shown in Fig. 11(b).

Various parameters can be derived from the profiles calculated by TRANSP. The Alfvén speed and frequency profiles are plotted in Fig. 12. They are defined as

$$v_{\text{Alfvén}} = \frac{B_{\text{TF}}}{\sqrt{4\pi m_{\text{H}}(2n_{\text{D}} + 3n_{\text{T}} + 2n_{\text{D-beam}} + 3n_{\text{T-beam}} + 4n_{\alpha} + 12n_{\text{imp}})}}$$

$$\omega_{\text{Alfvén}} \approx \frac{v_{\text{Alfvén}}}{2q\psi R}$$

The trajectory in time of  $\langle \beta_\alpha \rangle$  versus the ratio  $v_{\text{alpha}}(0)/v_{\text{Alfvén}}(0)$  of the birth alpha speed to the Alfvén speed at  $x = 0$  is shown in Fig. 13. This ratio achieves its peak value during the stationary phase and then rapidly decreases after the NBI as the density decreases. TAE modes are expected to be excited during this ramp-down phase [1].

Many of the profiles are fitted well by a sum of a Gaussian and a power of  $1 - x^2$ . A summary of simple fits to the central values ( $x < 0.5$ ) of several of the profiles using either a Gaussian or a power of  $1 - x^2$  is given in the Table III.

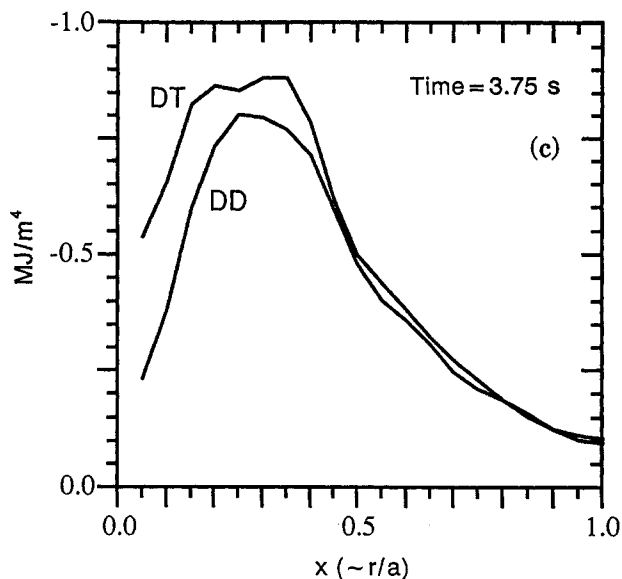
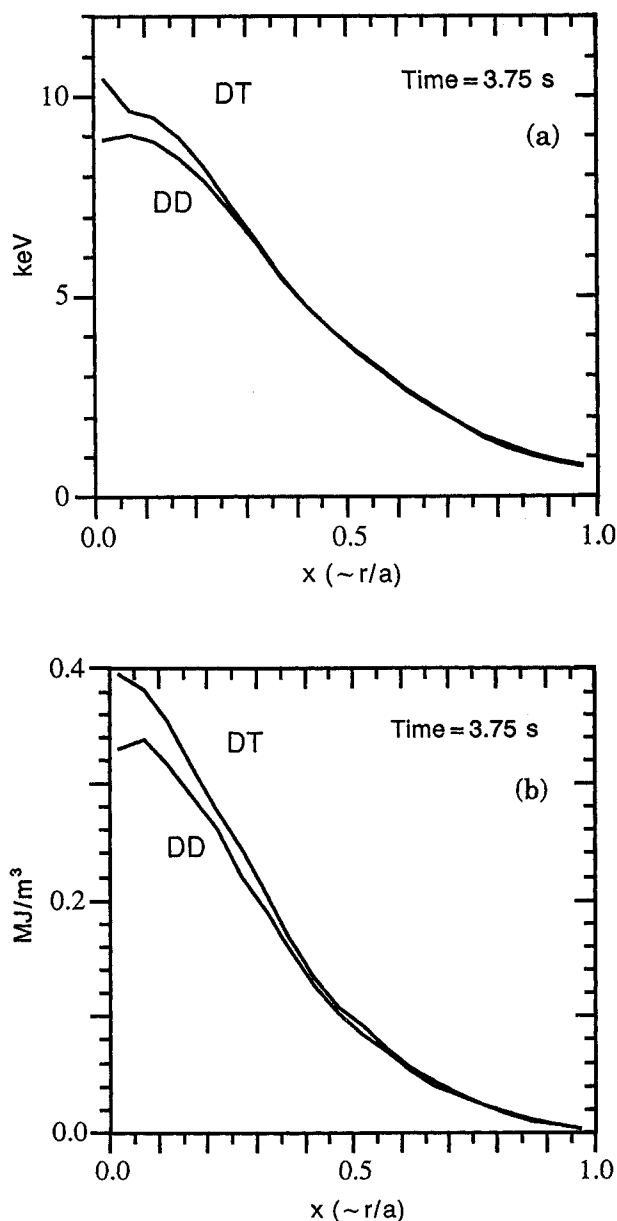


FIG. 9. Comparison of the DD and equivalent DT profiles of (a)  $T_e$ , (b) total pressure, and (c) gradient of the total pressure versus  $x$ .

## 5. DISTRIBUTIONS

Both Monte Carlo and Fokker-Planck methods were used to generate the distribution functions

$$f \equiv \frac{dn}{dE d\lambda}$$

of fast ions in the laboratory frame. The independent variables are  $x$ , pitch angle  $\lambda$  and energy  $E$ . Plots of integrals of the distributions over  $E$  or  $\lambda$  from the Monte Carlo simulation are given in Figs 14–16 at 3.75 s, during the relatively stationary phase of the NBI.

The distributions in energy and  $x$  show an increased peaking at low energies at large  $x$ . This is caused partly by the arbitrary separation of fast ions and thermal ions at energies of  $(3/2)T_D$ . The pitch angle distributions of the beam ions and the alpha distributions are peaked at forward and backward pitch angles  $\lambda = -1$  and  $+1$  since the ions with  $\lambda \sim 0$  have larger excursions into regions of large  $x$  with higher probability of being lost. The distributions are also skewed towards positive pitch angles, especially for alphas at large  $x$ . This is caused by preferential losses of counter-streaming ions. One consequence of this is that the profiles of the average rotation of fast ions are peaked with co-rotation at large  $x$ , as shown in Fig. 17. A simulation was performed with the total plasma current increased to 8 MA to compare the  $\lambda$  distributions. The alpha distributions for this extrapolation are much flatter, because of smaller banana widths.

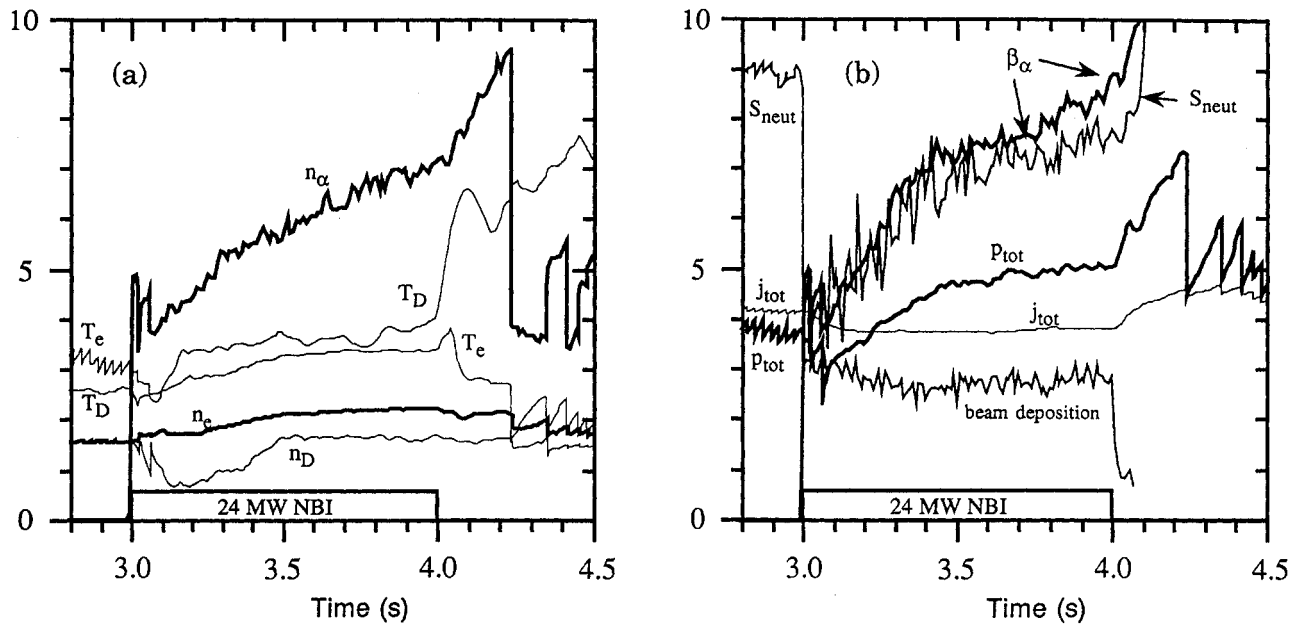


FIG. 10. Peakedness of various profiles including DT neutron emission, fast alphas,  $\beta_\alpha$  and total pressure.

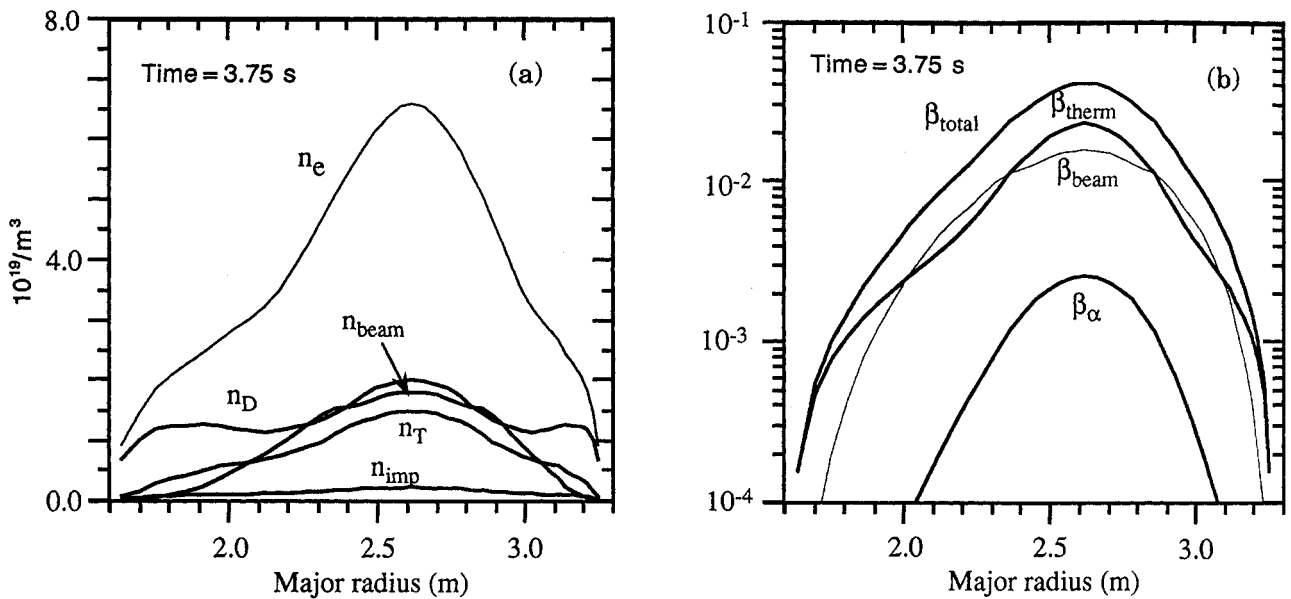


FIG. 11. Profiles versus major radius of (a) densities, (b) components of toroidal beta including the alpha particle component  $\beta_\alpha$ .

There is considerable noise in the distributions due to the Monte Carlo sampling. The noise was reduced by sampling 4000 beam ions and 4000 alpha particles. Also, the sampling was averaged over a time range of 200 ms. The Fokker-Planck runs do not have sampling noise, and

so the D and T distributions are similar to those in Figs 14–16, except for being smoother and differing in the low energy regions because of the different thermalization models used.

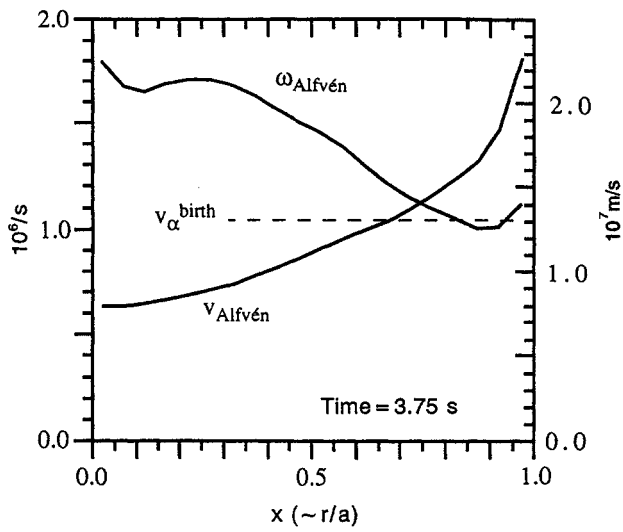


FIG. 12. Profiles of Alfvén speed and frequency.

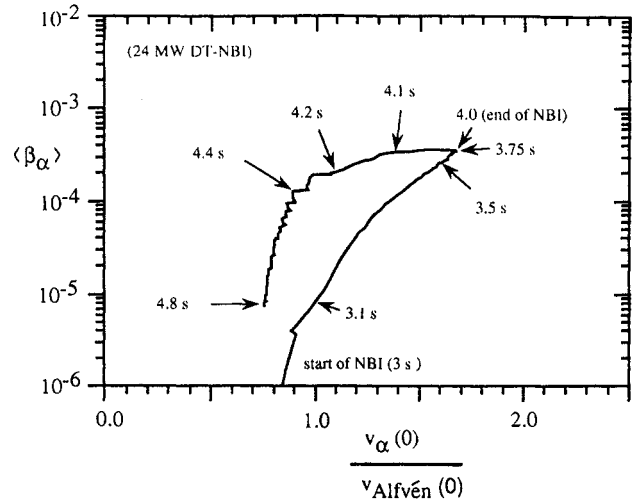


FIG. 13. Trajectory of  $\langle \beta_\alpha \rangle$  versus  $v_\alpha(0)/v_{\text{Alfvén}}(0)$ .

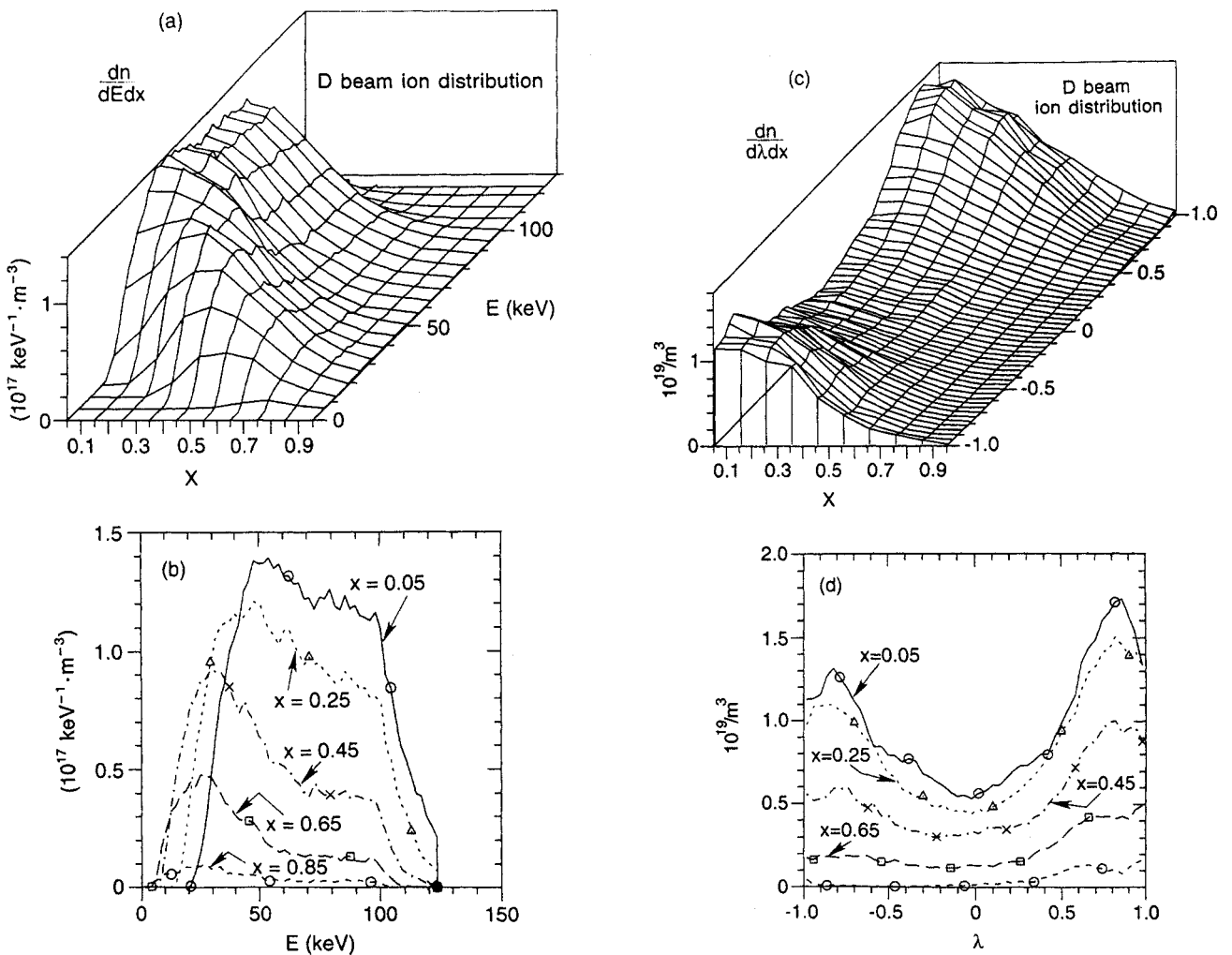


FIG. 14. Integrals over (a), (b) pitch angle, and (c), (d) energy of the fast D beam ion distribution computed with the Monte Carlo option at 3.75 s.

TABLE III. SIMPLE FITS TO CENTRAL VALUES OF SELECTED PARAMETERS

Fast ions	Fit to $F$	Fit to $\ln F, E < E_0$	Fit to $\ln E, E > E_0$
	$E_{crit}$ (keV)	$T_{eff}$ (keV)	$T_{eff}$ (keV)
D	71	90	14
T	100	110	12
$\alpha$	750	1300	65

Plots for the pitch angle integrated distributions and for the thermal Maxwellian distributions

$$f_{Maxwell} \sim \sqrt{E} \exp[-E/T]$$

at 3.75 s at the plasma centre are shown in Fig. 18. The Maxwellian components of the D and T distributions integrate to the central thermal densities,  $2.0 \times 10^{19}/m^3$  and  $1.5 \times 10^{19}/m^3$ , respectively. Although the thermal alpha density was not modelled in the TRANSP simulations discussed here, the alpha thermalization rate is predicted. The central alpha thermalization rate is very small ( $< 10^{17} m^{-3} \cdot s^{-1}$ ) up to 3.75 s, and increases rapidly after this time. The time integral of the central rate to 3.75 s is  $6 \times 10^{15}/m^3$ . This value was used to normalize the Maxwellian distribution shown in Fig. 18(c). After the NBI, the peak value rises to  $1.5 \times 10^{17}/m^3$ . Corresponding results from the Fokker-Planck simulation are shown in Fig. 19. These distributions differ from those in Figs 18(a) and (b) in the region of 20–40 keV, because of the different thermalization treatment.

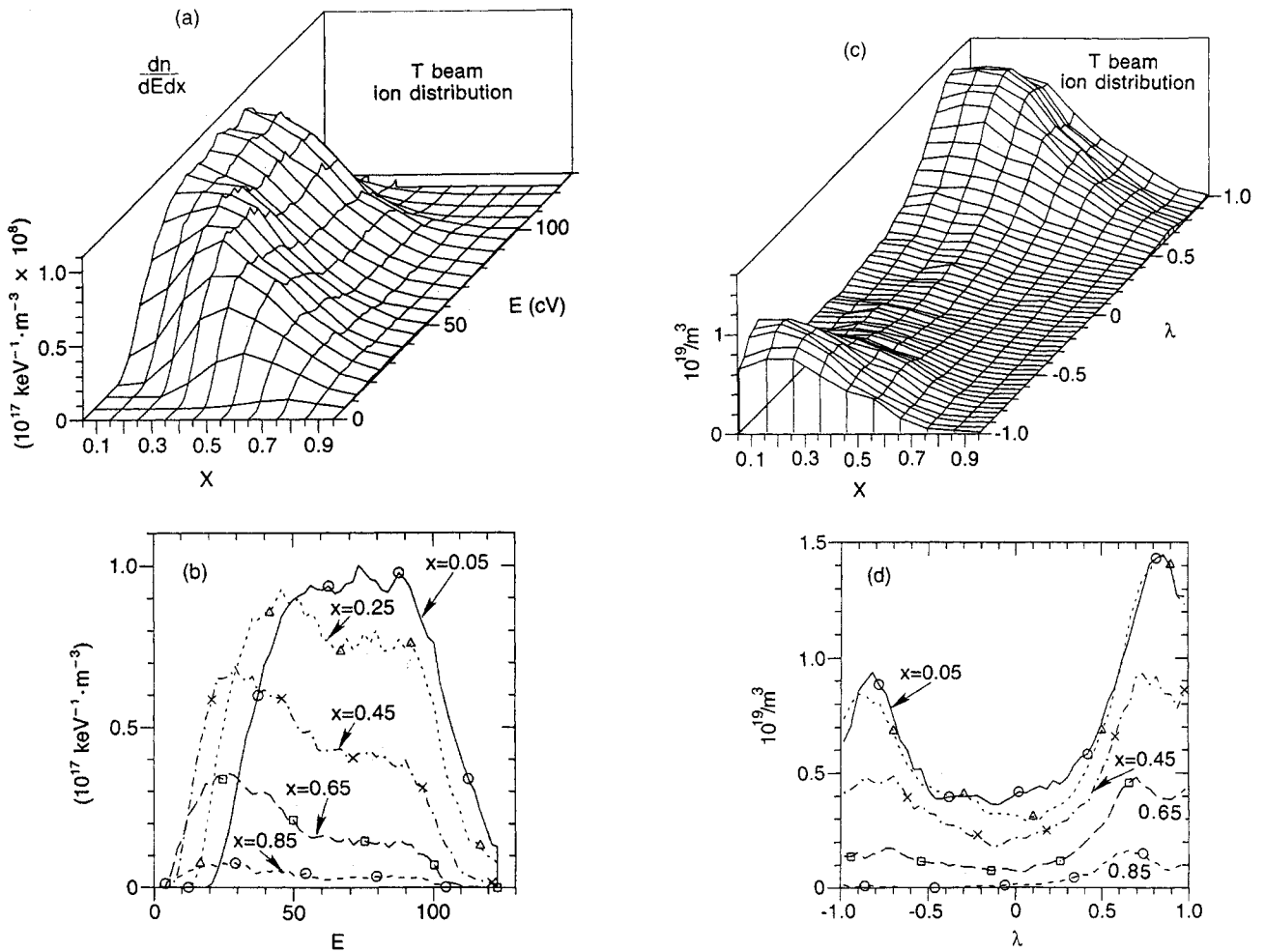


FIG. 15. Integrals over (a), (b) pitch angle and (c), (d) energy of the fast T beam ion distribution computed with the Monte Carlo option at 3.75 s.

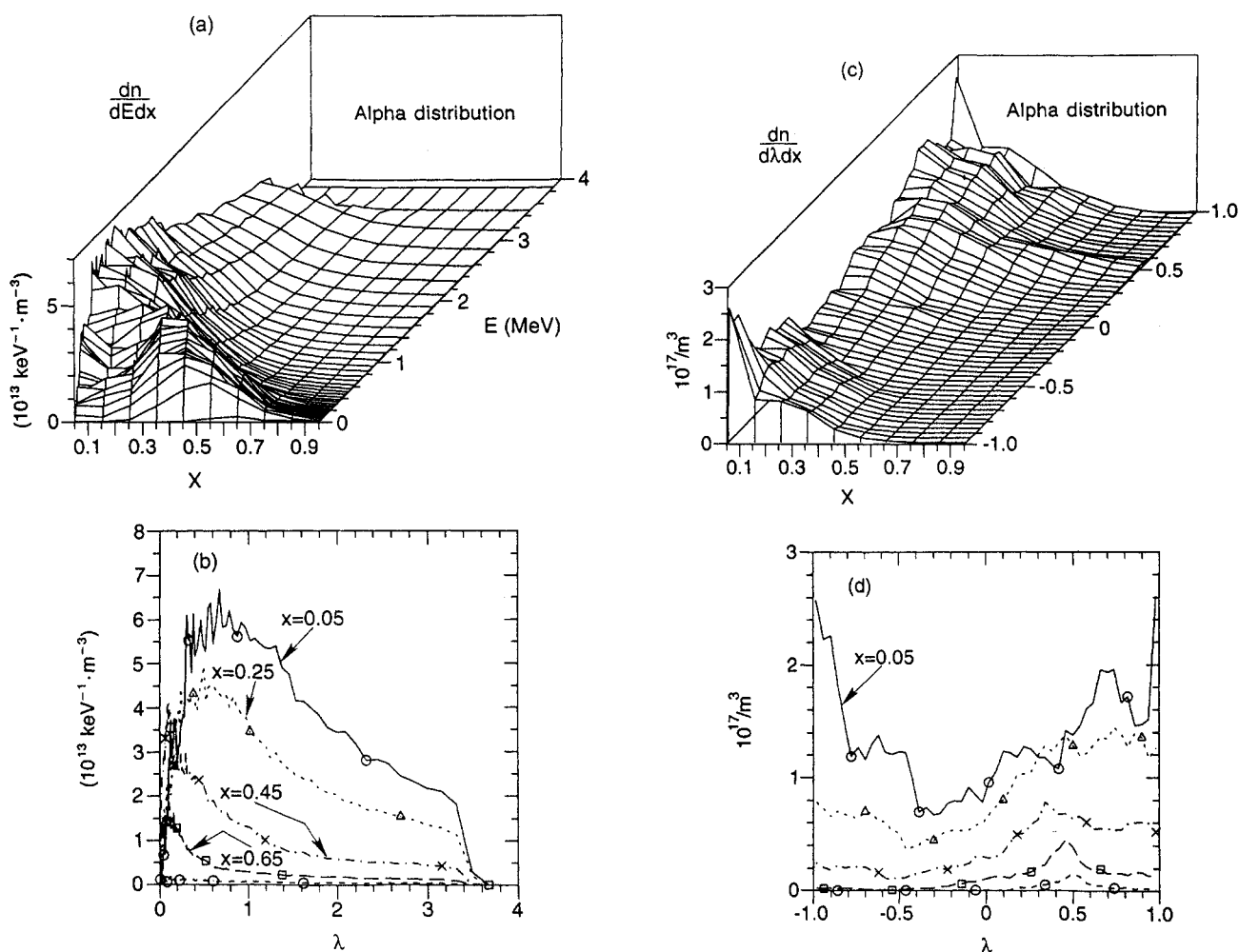


FIG. 16. Integrals over (a), (b) pitch angle and (c), (d) energy of the fast alpha distribution computed with the Monte Carlo option at 3.75 s.

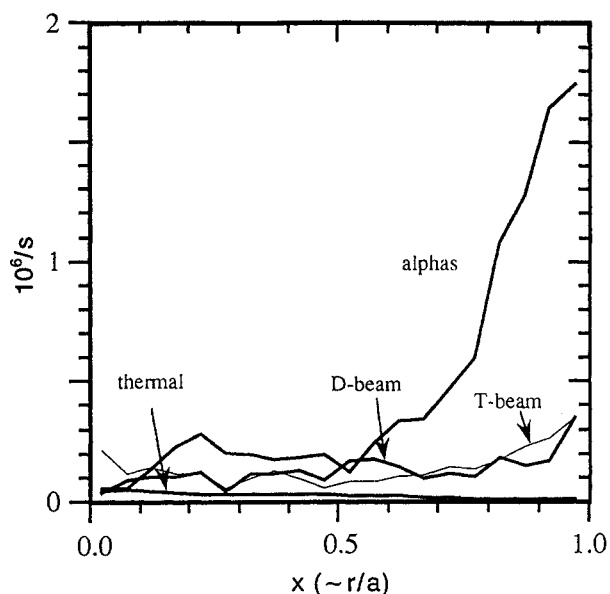


FIG. 17. Profiles of fast ion toroidal rotations.

Plots and fits to the pitch angle integrated distributions at the plasma centre, normalized as

$$F \equiv \frac{f}{\sqrt{E}}$$

are given in Fig. 20. In the  $T_D \sim 0$  approximation, the relatively flat middle region below the birth energy is predicted to decrease as

$$F \sim [E^{1.5} + E_{crit}^{1.5}]^{-1}$$

where  $E_{crit}$  is the critical energy [19]. The values of  $E_{crit}$  in the steady state are predicted to be  $\sim 20T_e$  for D beam ions and  $40T_e$  for alphas (using  $\ln \Lambda_e = 17$  and  $\ln \Lambda_{ion} = 23$ ). The values of these quantities at the centre are 205 and 409 keV, respectively. The fits to the distributions yield the cut-off energies shown in Table IV. These are lower than the values given above. The beam ion distributions are complicated by the high values of  $T_D$  and by the presence of the half and third NBI energy components.

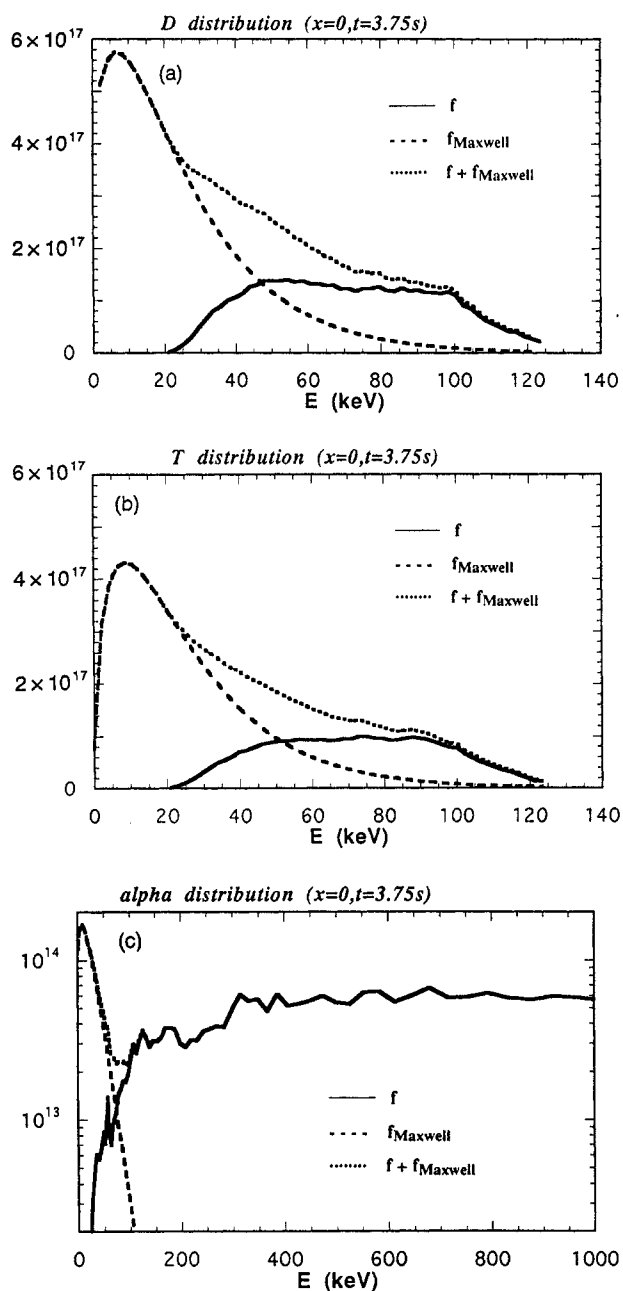


FIG. 18. Integrals over pitch angle of the central distribution  $f$ , the thermal distribution  $f_{\text{Maxwell}}$ , and their sum versus  $E$  from the Monte Carlo run of the fast (a)  $D$  ions, (b)  $T$  ions, and (c) alpha particles. The integrals of  $f_{\text{Maxwell}}$  give the central densities of the thermal  $D$ ,  $T$  and of the alpha ash estimated from the alpha thermalization rate.

An effective temperature  $T_{\text{eff}}$  can be deduced by fitting  $\ln F$  above the creation energies,  $E_0$  [20]. This temperature is a weighted average of  $T_D$  and  $T_e$ , depending on  $E_{\text{crit}}$ . Plots and fits are shown in Fig. 21. Fit parameters are shown in Table IV.

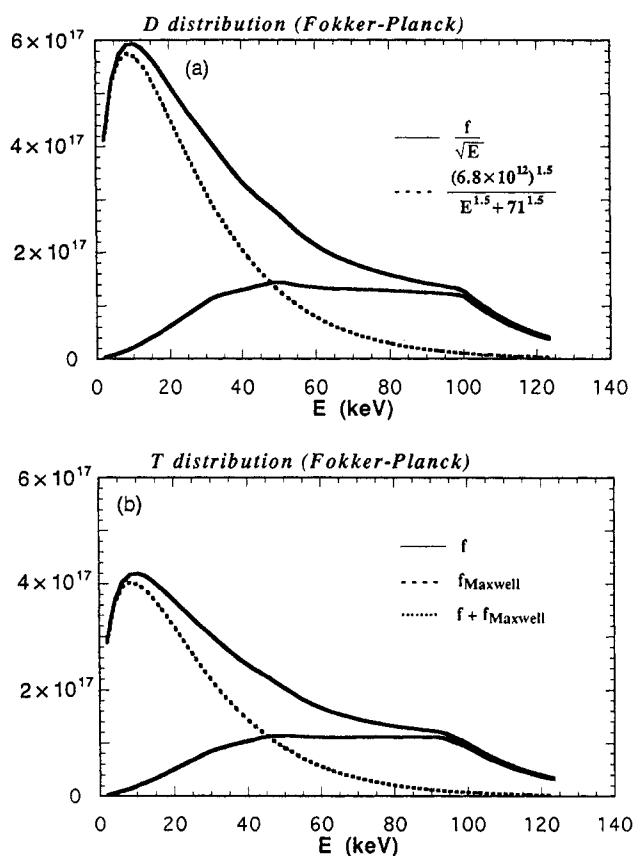


FIG. 19. Integral over pitch angle of the central distribution  $f$ , the thermal distribution  $f_{\text{Maxwell}}$ , and their sum versus  $E$  from the Fokker-Planck run of the fast (a)  $D$  ions and (b)  $T$  ions.

The distribution for the alphas evolves considerably during the discharge, even during the relatively stationary phase of the last 0.5 s of NBI. Early in the NBI the distribution versus energy is hollow, peaked near the birth energy. The fits for the central  $\ln F$  versus energy at several times — 3.6 s, just after the start of the stationary phase, and 4.0 s, just before the termination of the NBI — are compared with the value at 3.75 s in Fig. 22. The distributions become more Maxwellian at late times.

TABLE IV. FITS TO THE FAST ION DISTRIBUTIONS

Parameter	Gaussian fit $a \exp\{-(x/b)^2\}$		Power fit $a(1-x^2)^b$	
	$a$	$b$	$a$	$b$
$\beta$	0.040	0.41	0.040	5.6
$\beta_\alpha$	0.0026	0.33	0.0025	8.3
$n_\alpha$	$1.8 \times 10^{17}/\text{m}^3$	0.36	$1.8 \times 10^{17}/\text{m}^3$	7.3

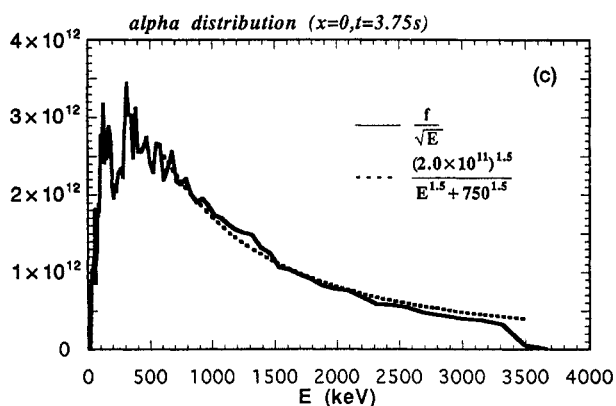
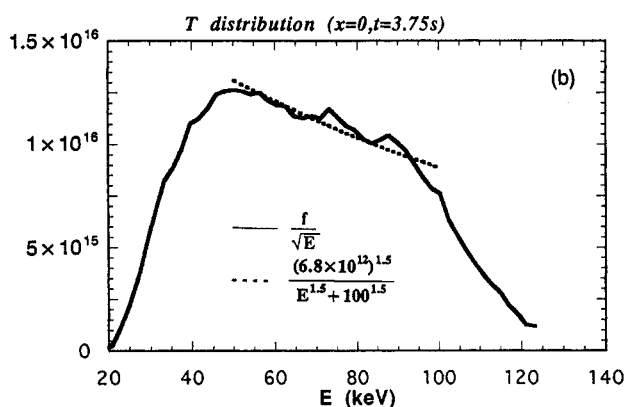
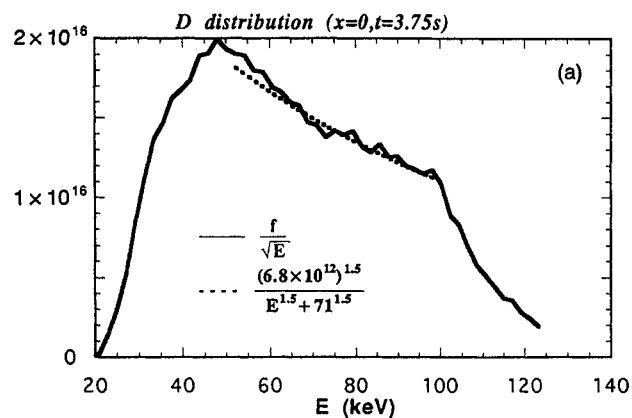


FIG. 20. Profiles and fits to  $F \equiv f/\sqrt{E}$  at  $x = 0$  from the Monte Carlo run of the fast (a) D beam ions, (b) T beam ions, and (c) alpha particles.

## 6. SUMMARY

TRANSP results for simulations of a TFTR DT supershot are given. They are based on a D-only supershot which was chosen since it is reproducible, has a high neutron yield, a long duration of stationary conditions, and appears to have a sufficient margin of stability to accomo-

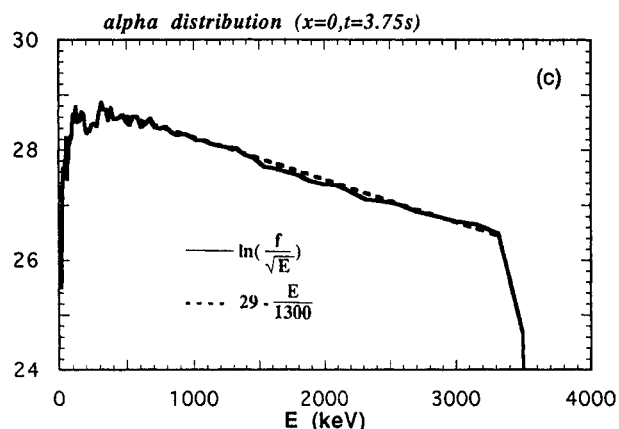
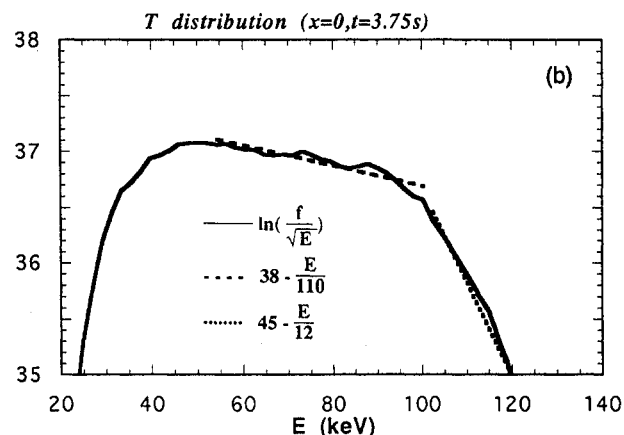
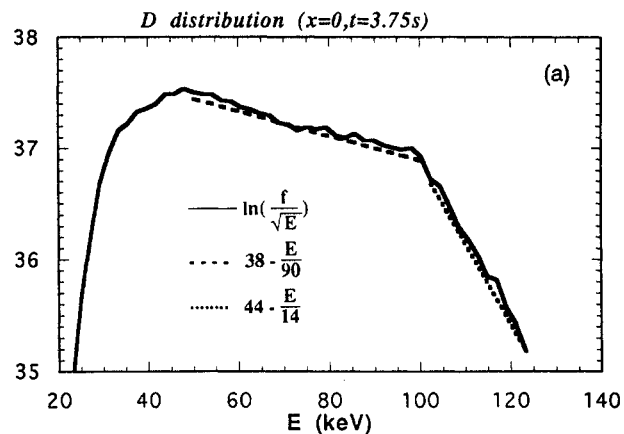


FIG. 21. Profiles and fits to  $\ln(f/\sqrt{E})$  at  $x = 0$  from the Monte Carlo run of the fast (a) D beam ions, (b) T beam ions, and (c) alpha particles.

date the increased pressure expected in DT. The simulation yields peak values of  $\beta_{\text{norm}} = 1.99$ , fusion power,  $P_{\text{DT}} = 5.6$  MW, and normalized fusion yield  $Q_{\text{DT}} = 0.23$ . The alpha-electron heating is predicted to be 1 MW, and the alpha power loss to the limiters is predicted to be small ( $< 10\%$  of this heating power).

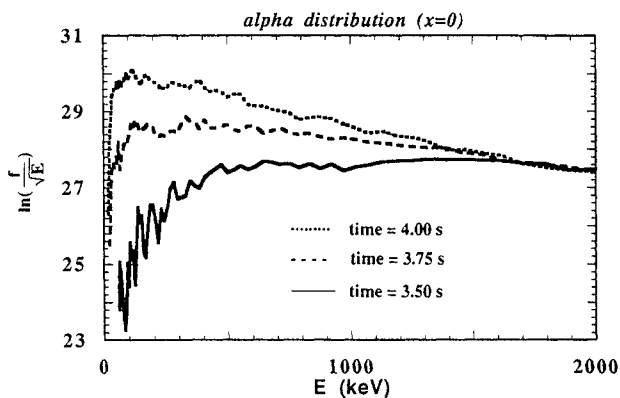


FIG. 22. Comparisons of  $\ln(f/\sqrt{E})$  for alpha particles at  $x = 0$  for different times.

Parameters and fits are given during the relatively stationary phase. Both the Monte Carlo and the Fokker-Planck options are used to calculate beam ion parameters, and the Monte Carlo option is used to calculate fast alpha parameters. The Monte Carlo option has a more complete model, including orbit width effects and beam-beam charge exchange recapture, except for the thermalization, and generally gives lower fusion rates.

Distributions versus position, energy and pitch angle are given. The D and T beam ion distributions are relatively constant during the relatively stationary phase of the NBI. The 1/2 and 1/3 energy components complicate the distribution, so it does not obey a standard slowing down distribution from a monoenergetic source. The alpha distributions evolve during this phase since the slowing down times are long. The alpha distributions in pitch angle are peaked at forward and backward pitch angles.

#### ACKNOWLEDGEMENTS

The author wishes to thank C.Z. Cheng, G. Hammett, S. Kishore, D. McCune, D. Mikkelsen, S. Sabbagh and S.J. Zweben for helpful comments, and M.G. Bell,

C. Bush, K. Hill, D. Jassby, L. Johnson, H. Park, D. Mansfield, A. Ramsey, G. Taylor, J. Schivel and E. Synakowski for measurements. The work was supported by USDOE Contract No. DE-AC02-76-CHO-3073.

#### REFERENCES

- [1] BUDNY, R.V., et al., Nucl. Fusion **32** (1992) 429.
- [2] CHENG, C.Z., Phys. Fluids B **3** (1991) 2463; CHENG, C.Z., et al., in Plasma Physics and Controlled Nuclear Fusion Research 1992 (Proc. 14th Int. Conf. Würzburg, 1992), Vol. 2, IAEA, Vienna (1993) 51.
- [3] BUDNY, R., et al., in Controlled Fusion and Plasma Physics (20th Eur. Conf. Lisbon, 1993), Vol. 17C, Part I, European Physical Society, Geneva (1993) 767.
- [4] CHANG, Z., et al., Transport effects of low ( $m, n$ ) MHD modes on TFTR supershots, to be published in Nuclear Fusion.
- [5] McGUIRE, K., et al., Phys. Rev. Lett. **50** (1983) 891.
- [6] GOLDSTON, R., et al., J. Comput. Phys. **43** (1981) 61.
- [7] STRACHAN, J.D., et al., Nucl. Fusion **21** (1981) 67.
- [8] HAMMETT, G.W., Fast Ion Studies of Ion Cyclotron Heating in the PLT Tokamak, PhD Dissertation, University Microfilms No. GAX86-12694, Princeton (1986).
- [9] BOIVIN, R.L., et al., Nucl. Fusion **33** (1993) 449.
- [10] ZWEBEN, S.J., et al., in Plasma Physics and Controlled Nuclear Fusion Research 1992 (Proc. 14th Int. Conf. Würzburg, 1992), Vol. 1, IAEA, Vienna (1993) 363.
- [11] ZWEBEN, S.J., et al., Nucl. Fusion **30** (1990) 1551.
- [12] HEIDBRINK, W.W., et al., Nucl. Fusion **34** (1994) 535.
- [13] McCAULLEY, S.J., et al., Fast-Ion Diffusion Measurements From Radial Triton Burn-Up Studies, Rep. PPPL-2932, Princeton Plasma Physics Laboratory, Princeton, NJ.
- [14] SABBAGH, S., Columbia University, New York, USA, personal communication (1993).
- [15] DELUCIA, J., et al., J. Comput. Phys. **37** (1980) 183.
- [16] PHILLIPS, M.W., et al., Nucl. Fusion **28** (1988) 1499.
- [17] MANICKAM, J., Princeton Plasma Physics Laboratory, Princeton, NJ, personal communication (1993).
- [18] GRIMM, R.C., et al., J. Comput. Phys. **49** (1983) 94.
- [19] JASSBY, D.L., Nucl. Fusion **17** (1977) 309.
- [20] FIORE, C.L., et al., Nucl. Fusion **28** (1988) 1315.

(Manuscript received 13 September 1993

Final manuscript received 27 April 1994)